A generalised Phan–Thien—Tanner model

Journal of Non-Newtonian Fluid Mechanics 269 (2019) 88–99

Contents lists available at ScienceDirect

Journal of Non-Newtonian Fluid Mechanics

journal homepage: www.elsevier.com/locate/jnnfm

A generalised Phan–Thien—Tanner model

L.L. Ferrás[a,*], M.L. Morgado[b], M. Rebelo[c], Gareth H. McKinley[d], A.M. Afonso[e]

[a] CMAT - Centro de Matemática and Departamento de Matemática, Universidade do Minho, Guimarães 4800-058, Portugal
[b] CEMAT, Instituto Superior Técnico, Universidade de Lisboa & Department of Mathematics, University of Trás-os-Montes e Alto Douro, UTAD, Vila Real, Portugal
[c] Centro de Matemática e Aplicações (CMA) and Departamento de Matemática, Faculdade de Ciências e Tecnologia, Universidade NOVA de Lisboa, Quinta da Torre, Caparica 2829-516, Portugal
[d] Department of Mechanical Engineering, Massachusetts Institute of Technology, Cambridge, MA 02139 USA
[e] Centro de Estudos de Fenómenos de Transporte, Departamento de Engenharia Mecânica, Faculdade de Engenharia da Universidade do Porto, Rua Dr. Roberto Frias s/n, Porto 4200-465, Portugal

ARTICLE INFO

Keywords:
Viscoelastic fluids
PTT Model
Mittag–Leffler
Fitting rheological data

ABSTRACT

In this work we propose a novel generalised form of the Phan–Thien and Tanner (PTT) model by considering a new functional form of the nonlinear expression characterizing the destruction of physical network junctions and entanglements. This new function of the trace of the stress tensor is given by the generalized Mittag–Leffler function, and contains the familiar exponential form of the original Phan–Thien and Tanner model as a limiting case, but affords additional fitting flexibility through the inclusion of one or two additional fitting constants. We perform fits to experimental data in shear and extension and show that this generalized expression allows a better description of the rheological responses for a range of complex materials such as polymer melts and semidilute polymer solutions. By using an appropriate information criterion, we also demonstrate that the resulting generelized model remains parsimonious but provides improved fits of real world data.

1. Introduction

In 1977 Nhan Phan–Thien and Roger I. Tanner proposed a new constitutive equation (PTT) derived from a Lodge–Yamamoto type of network theory for polymeric fluids, see Fig. 1(a), in which the network junctions are not assumed to move strictly as points of the continuum but instead they are allowed a certain *effective slip* as well as a rate of destruction that depends in the state of stress in the network [1]. The model can then be expressed (for the isothermal case) by the constitutive expression:

$$K(\tau_{kk})\boldsymbol{\tau} + \lambda\overset{\nabla}{\boldsymbol{\tau}} = 2\eta_p\mathbf{D}, \quad K(\tau_{kk}) = 1 + \frac{\varepsilon\lambda}{\eta_p}\tau_{kk} \tag{1}$$

where $\mathbf{D}$ is the rate of deformation tensor, $\boldsymbol{\tau}$ is the stress tensor, λ is a relaxation time, η_p is the polymeric viscosity, τ_{kk} is the trace of the stress tensor, ε represents the extensibility parameter and $\overset{\nabla}{\boldsymbol{\tau}}$ represents the Gordon–Schowalter derivative defined as

$$\overset{\nabla}{\boldsymbol{\tau}} = \frac{\partial\boldsymbol{\tau}}{\partial t} + (\mathbf{u}\cdot\nabla)\boldsymbol{\tau} - (\nabla\mathbf{u})^T\cdot\boldsymbol{\tau} - \boldsymbol{\tau}\cdot(\nabla\mathbf{u}) + \xi(\boldsymbol{\tau}\cdot\mathbf{D} + \mathbf{D}\cdot\boldsymbol{\tau}). \tag{2}$$

Here, $\mathbf{u}$ is the velocity vector, $\nabla\mathbf{u}$ is the velocity gradient and the parameter ξ $(0\le\xi\le1)$ accounts for the slip between the molecular network and the continuous medium.

In 1978, Phan–Thien proposed a slightly more complex model that could behave more realistically in strong flows in which certain strain components grow exponentially in time [2,3]. He proposed that an exponential function form would be quite adequate to represent the rate of destruction of junctions, see Fig. 1(b), leading to the following model

$$\exp\left(\frac{\varepsilon\lambda}{\eta_p}\tau_{kk}\right)\boldsymbol{\tau} + \lambda\overset{\nabla}{\boldsymbol{\tau}} = 2\eta_p\mathbf{D}. \tag{3}$$

In fact, Phan–Thien [2] showed that the exponential function could provide a better fit to experimental data, especially when strong flows are being considered (for example, extensional flow). He also suggested the parameter ε to be of order 0.01.

In this work we further extend the work of Phan–Thien [2] by considering an even more general function for the rate of destruction of junctions. The function considered is based on the generalized Mittag–Leffler function,

$$E_{\alpha,\beta}(z) = \sum_{k=0}^{\infty}\frac{z^k}{\Gamma(\alpha k+\beta)} \tag{4}$$

that reduces to the exponential function when $\alpha=\beta=1$ (we consider real and positive α, β). When $\beta=1$ we obtain the original one-parameter Mittag–Leffler function, E_α [6]. Here, Γ is the Gamma function given

* Corresponding author.
E-mail addresses: luislimafr@gmail.com (L.L. Ferrás), luisam@utad.pt (M.L. Morgado), msjr@fct.unl.pt (M. Rebelo), gareth@mit.edu (G.H. McKinley), aafonso@fe.up.pt (A.M. Afonso).

https://doi.org/10.1016/j.jnnfm.2019.06.001
Received 25 May 2018; Received in revised form 15 April 2019; Accepted 5 June 2019
Available online 8 June 2019

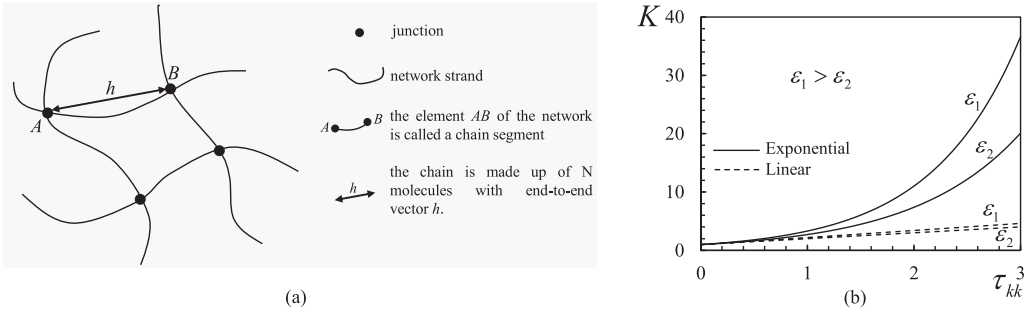

Fig. 1. (a) Lodge–Yamamoto network. The polymer liquid consists of polymer segments connected by junctions, and constantly changes its topology. Each chain is made of *N submolecules* with a common end-to-end vector *h*. (b) Exponential form of function *K* that was intuitively suggested by Nhan Phan–Thien [2] to describe the rate of destruction of junctions, considering two different values of ε (denoted by ε_1 and ε_2). We also plot the linear form of $K(\tau_{kk})$ for comparison.

by:

$$\Gamma(t) = \int_0^\infty x^{t-1} e^{-x} dx. \tag{5}$$

The Mittag–Leffler function given in Eq. (4) arises (as a function of time) in fractional relaxation models for viscoelastic liquids [4]. Usually we think of classical relaxation phenomena described in terms of the exponential function $\phi(t) = e^{-t/T}$ (with T a characteristic time scale) often referred to as Maxwell–Debye relaxation. This model is far from perfect for real materials, since in many systems, large deviations from this classical mono-exponential case are observed. Such systems can be well modeled, for example, by the Kohlrausch–Williams–Watts or stretched exponential function $\phi(t) = e^{-(t/T)^b}$ $(0 < b < 1)$. In 2002 Metzler and Klafter [5] derived a generalisation of this relaxation function, using fractional calculus which naturally gives rise to the Mittag–Leffler function $E_{\alpha,1}(z) = E_\alpha(z)$. The relaxation is then given by $\phi(t) = E_\alpha(-(t/T)^\alpha)$, and, for small values of the argument $(t/T \ll 1)$ we have $E_\alpha(-(t/T)^\alpha) \approx e^{-(t/T)^\alpha}$. The resulting fractional viscoelastic constitutive models allow a better fit to rheological data and at the same time make use of a smaller number of parameters, when compared, for example, with multi-mode approaches [4].

Based on these considerations, the Mittag–Leffler function seems to be a good candidate to better describe the rate of destruction of junctions and the behavior of complex materials. Therefore, we propose a new function describing network destruction that can be written as,

$$K(\tau_{kk}) = \Gamma(\beta) E_{\alpha,\beta}\left(\frac{\varepsilon\lambda}{\eta_p}\tau_{kk}\right) \tag{6}$$

where the normalization $\Gamma(\beta)$ is used to ensure that $K(0) = 1$ for all choices of β. In the case that α and β are real and positive, the series in (4) converges for all values of the argument z. It should be remarked that the parameter ε in Eq. (6) cannot be compared directly to the one used in the original PTT model when α and β are different than 1. This can be easily seen by performing a series expansion of e^z and $\Gamma(\beta)E_{\alpha,\beta}(z)$, for $z \ll 1$ [6],

$$e^z \cong \sum_{k=1}^{N} \frac{z^{k-1}}{(k-1)!} + \mathcal{O}(z^N), \tag{7}$$

$$\Gamma(\beta)E_{\alpha,\beta}(z) \cong \Gamma(\beta) \sum_{k=1}^{N} \frac{z^{k-1}}{\Gamma(\alpha(k-1)+\beta)} + \mathcal{O}(z^N). \tag{8}$$

The parameters α and β will influence the behavior of the Mittag–Leffler function, and therefore, for the same value of ε the two functions will provide different values, unless $\alpha = \beta = 1$, so that $E_{\alpha,\beta}(z) = e^z$.

Fig. 2 shows the variation of $\Gamma(\beta)E_{\alpha,\beta}(z)$ for several different values of α and β. We observe that different rates of increase in the destruction rate are obtained, with decreasing values of α and β. Note the comparison with the exponential function ($\alpha = \beta = 1$). It is evident that the Mittag–Leffler function allows a wider range of variation in the rates of destruction of network junctions and thus more flexibility in fitting experimental data.

It should be remarked that Phan–Thien [2], when proposing the exponential PTT model, stated intuitively that the unknown function of the trace of the stress tensor could be roughly expected to follow an exponential behavior, because the greater the extension of each network strand, the higher the resulting destruction rate. Assuming the existence of a linear elastic response at small strains, we expect a linear variation in this function for small deformations, but, as the deformation increases, a more abrupt variation of the rate of destruction is expected to occur, until a critical segment length is achieved. Since this is a continuum model, the exponential function brings information from the microstructural scales into the continuum model; therefore, the more realistic the description of the microscopic scale, the better we should expect the continuum model to describe real data. A generalization of the exponential function would then allow, in principle, improved fitting of measured rheological responses. Now the question is: how to relate the new parameters α and β to the physics of the process? Note that when proposing a new function of the trace of the stress tensor (linear, exponential and generalized versions), we are already making assumptions on the structure of the material.

Phan–Thien [2] introduces the simple material specific *constant* ε (typically found to be of order 0.01). The effect of this parameter on the rate of destruction is considerable, and, it turns out that the steady-state Trouton viscosity at large stretch rates is inversely proportional to ε [2]. The introduction of two additional parameters in our general expression Eq. (6) will result in the Trouton viscosity varying with α and β.

The parameters α and β change the shape of the destruction rate function, and therefore, we can no longer say that ε will always remain of order 0.01. Also, for highly branched materials such as low-density polyethylene (LDPE), the exponential function may not be sufficient to deal with the microstructural complexity of the material (that being one of the reasons for the creation of the *pom-pom* model. This model also takes into account the different relaxation times for orientation and stretch). Therefore, we may conclude that when we change the parameters α and β it means that we are adopting a more complex and more flexible function of the trace of the stress tensor.

A way to verify that the new model (with extra fitting parameters) provides a better description of real experimental data is to use an appropriate statistical measure of the fitting quality that penalizes the addition of extra parameters. This is possible using, for example, the Akaike information criterion (AIC), proposed by Hirotugu Akaike in 1973 [7,8]. His measure, provides a framework for rational model selection in the analysis of empirical data, allowing the selection of the most appropriate parsimonious model. The AIC provides a simple, effective, and objective means for the selection of an estimated *best approximating model* for data analysis and inference [9].

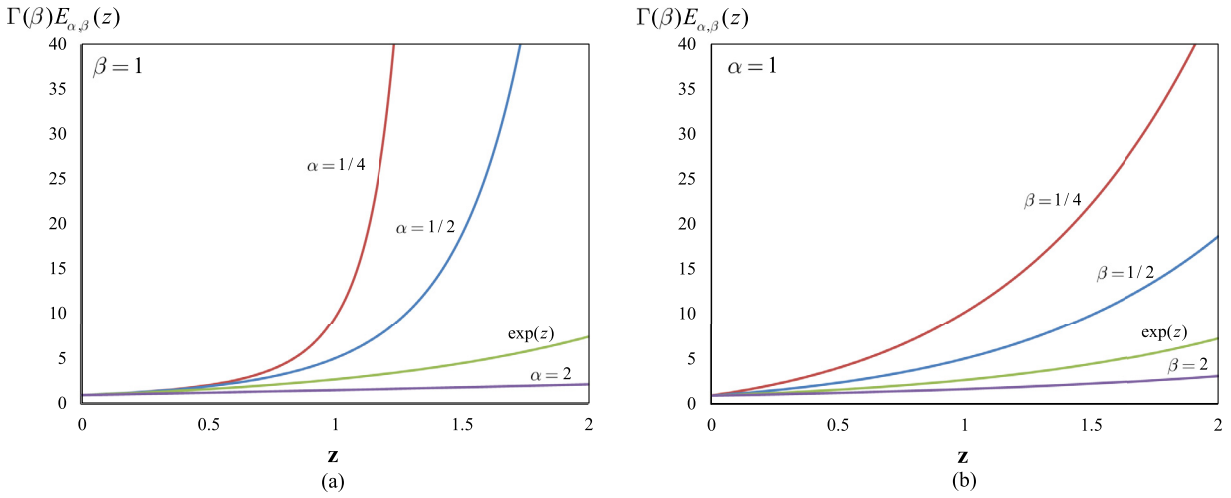

Fig. 2. Influence of α and β on the shape of $\Gamma(\beta)E_{\alpha,\beta}(z)$ where $z = \varepsilon\lambda\tau_{kk}/\eta_p$. (a) $\beta = 1$, (b) $\alpha = 1$. (The Mathematica software was used to plot this function.)

The AIC is given by:

$$AIC = N\ ln\left(\frac{RSS}{N}\right) + 2K, \tag{9}$$

where N is the number of observations, K is the number of estimated parameters plus 1, RSS is the residual sum of squares error - the minimized distance between the experimental data and the corresponding model prediction of the data. Note that the lower the AIC value, the *better* the model is. We use this measure to show that the addition of two additional model parameters (α and β) does not result in over fitting of typical rheological data and in fact improves the goodness of fit, and lowers the AIC value.

This work is organized as follows. In the next two Sections we present the governing equations for an isothermal incompressible fluid described by the generalised PTT (denoted gPTT) model and we present a fit to rheological data obtained in both steady and transient shear and extensional flows (shear viscosity, first normal stress coefficient and uniaxial extensional viscosity). In Section 4 we derive the analytical solution for the channel and pipe flows of a generalised simplified PTT (sPTT, with $\xi = 0$) fluid together with the semi-analytical solution for the full gPTT obtained with $\xi \neq 0$. We also consider the possibility of constitutive instabilities in the system dynamics due to non-monotonic variations in the steady flow curve for certain ranges of model parameters Section 5.

2. Governing equations

The equations governing the flow of an isothermal incompressible fluid are the continuity equation,

$$\nabla \cdot \mathbf{u} = 0 \tag{10}$$

and the momentum equation,

$$\rho\frac{D\mathbf{u}}{Dt} = -\nabla p + \nabla \cdot \boldsymbol{\tau} \tag{11}$$

together with the constitutive equation,

$$\Gamma(\beta)E_{\alpha,\beta}\left(\frac{\varepsilon\lambda}{\eta_p}\tau_{kk}\right)\boldsymbol{\tau} + \lambda\overset{\nabla}{\boldsymbol{\tau}} = 2\eta_p\mathbf{D}. \tag{12}$$

where p is the pressure, t the time and ρ the mass density. The Gordon–Schowalter derivative $\overset{\nabla}{\boldsymbol{\tau}}$ is given in Eq. (2) above. The quantity η_p/λ can also be recognized as the elastic modulus G of the polymeric network under equilibrium conditions.

3. Fit to experimental rheological data

In this Section, we are interested in showing that this new model provides a *better fit* to experimental rheological data (using an appropriate statistical measure of goodness of fit), and therefore, the full PTT model will be considered (Eq. (12) with $\xi \neq 0$).

3.1. Weak steady flows

In this Subsection we will consider steady simple shear flows, for which explicit expressions for the material functions can be easily found. Note that Phan–Thien [2] concluded that for weak flows (for example viscometric flows) the predictions of the exponential PTT model are insensitive to the values of ε.

Following the work of Alves et al. [10] and considering a simple plane shear flow aligned with the x-axis, the constitutive Eq. (12) reduces to:

$$K(\tau_{kk})\tau_{xx} = (2-\xi)(\lambda\dot{\gamma})\tau_{xy}, \tag{13}$$

$$K(\tau_{kk})\tau_{yy} = -\xi(\lambda\dot{\gamma})\tau_{xy}, \tag{14}$$

$$K(\tau_{kk})\tau_{xy} = \eta_p\dot{\gamma} + (1-\xi/2)(\lambda\dot{\gamma})\tau_{yy} - \frac{\xi}{2}(\lambda\dot{\gamma})\tau_{xx}, \tag{15}$$

where $\dot{\gamma}$ is the constant shear rate $\dot{\gamma} = |du/dy|$. The ratio of Eqs. (13) and (14) leads to the relationship $\tau_{yy} = -\tau_{xx}\xi/(2-\xi)$, and, its substitution in Eq. (15) together with τ_{xy} obtained from Eq. (13) and $K(\tau_{kk}) = \Gamma(\beta)E_{\alpha,\beta}(\frac{\varepsilon\lambda}{\eta_p}(\tau_{xx}+\tau_{yy}))$ leads to the following nonlinear equation for τ_{xx},

$$\Gamma^2(\beta)E_{\alpha,\beta}\left(\frac{\varepsilon\lambda}{\eta_p}\left(\frac{2-2\xi}{2-\xi}\right)\tau_{xx}\right)^2\tau_{xx} = (2-\xi)(\lambda\dot{\gamma})^2[\eta_p/\lambda - \tau_{xx}\xi]. \tag{16}$$

The shear stress τ_{xy} as a function of $\dot{\gamma}$ is obtained from Eq. (15), and is given by:

$$\tau_{xy}(\dot{\gamma}) = \frac{\eta_p\dot{\gamma} - \tau_{xx}Wi\xi}{\Gamma(\beta)E_{\alpha,\beta}\left(\frac{\varepsilon\lambda}{\eta_p}\left(\frac{2-2\xi}{2-\xi}\right)\tau_{xx}\right)} \tag{17}$$

with $Wi = \lambda\dot{\gamma}$, the Weissenberg number.

We can therefore obtain the viscometric material functions: the steady shear viscosity, $\eta(\dot{\gamma})$, and the first and second normal stress coefficients, $\Psi_1(\dot{\gamma})$ and $\Psi_2(\dot{\gamma})$, respectively, that are given by:

$$\eta(\dot{\gamma}) = \frac{\tau_{xy}(\dot{\gamma})}{\dot{\gamma}}, \tag{18}$$

$$\Psi_1(\dot{\gamma}) = \frac{\tau_{xx}-\tau_{yy}}{\dot{\gamma}^2} = \frac{2\tau_{xx}}{(2-\xi)\dot{\gamma}^2}, \tag{19}$$

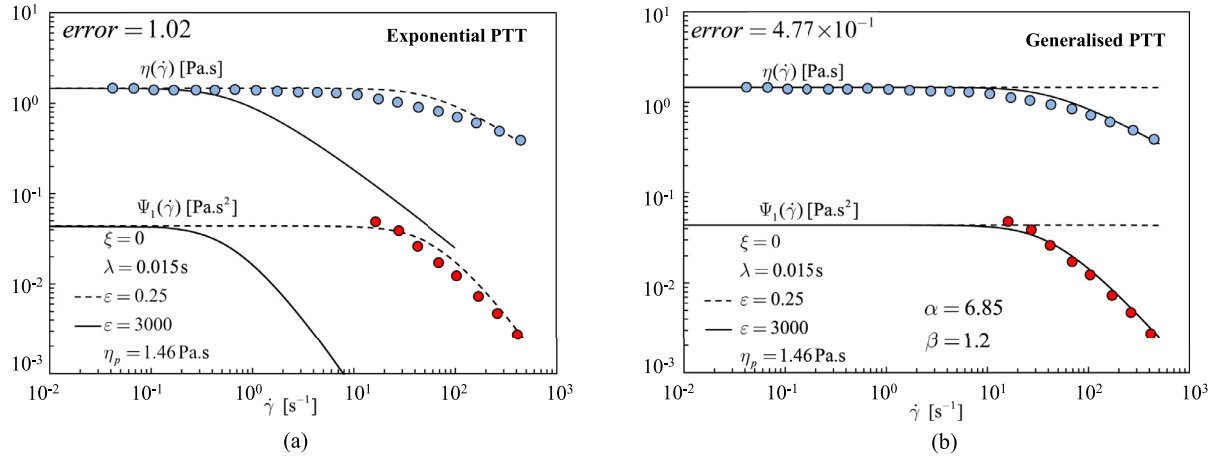

Fig. 3. Model fits to the shear viscosity and first normal stress difference data obtained by Quinzani et al. for a concentrated polymer solution [11]. Note that in the limit $Wi \ll 1$ we have $\lim_{\dot{\gamma}\to 0}\eta(\dot{\gamma}) \to \eta_p = G\lambda$.(a) Exponential PTT, (b) Generalised PTT. The symbols represent the experimental data and the full lines and dashed lines represent the fit obtained with each model for $\varepsilon = 3000, 0.25$, respectively. The *error* (Eq. (21)) was only computed for the best fit (dashed lines in (a) and solid lines in (b)).

$$\Psi_2(\dot{\gamma}) = \frac{-\xi\tau_{xx}}{(2-\xi)\dot{\gamma}^2}. \tag{20}$$

In order to test the ability of this new model to provide good fits to experimental rheological data, we have compared the fits obtained with the exponential and generalised PTT models, to the shear viscosity and first normal stress difference obtained experimentally in the work of Quinzani et al. [11]. The results are shown in Fig. 3. It should be recalled that in the new generalised PTT model the parameter ε can no longer be expected to have the same magnitude as the values obtained from the linear and exponential PTT models (when $\alpha = \beta = 1$).

To quantify the error incurred during the fitting process we will use a mean square error given by

$$error = \sum_{i=1}^{N_\eta}\left[\log\eta(\dot{\gamma})_i - \log\eta(\dot{\gamma})_{fit_i}\right]^2 + \sum_{j=1}^{N_{\Psi_1}}\left[\log\Psi_1(\dot{\gamma})_j - \log\Psi_1(\dot{\gamma})_{fit_j}\right]^2. \tag{21}$$

with N_η and N_{Ψ_1} the number of experimental points obtained for $\eta(\dot{\gamma})$ and $\Psi_1(\dot{\gamma})$, respectively.

A better fit was obtained for the new generalised model (Fig. 3), when compared to the original exponential PTT model. The total mean square error obtained for the exponential PTT model (1.02) is more than twice the error obtained for its generalised version (4.77×10^{-1}). The new model allows a better fit in the shear-thinning region at high shear rates. We have also used the Akaike Information Criterion given by Eq. (9) to evaluate the best approximating model for the available data and obtain values of $AIC_{\Psi_1} = -83.7$, $AIC_\eta = -66.4$ and $AIC_{\Psi_1} = -85.7$, $AIC_\eta = -78.2$ for the exponential and generalised PTT models, respectively. Lower values of AIC indicate a more likely approximation.

Although we were not initially expecting a better fit with the new model for weak shearing flows (due to the conclusions of Phan–Thien based on the exponential PTT model), it turns out that the rate-dependent variation of the rate of destruction of network junctions can still be felt in simple shear flows (by considering high α and ε values which changes the dominant balance of the terms in the equations for $\eta(\dot{\gamma})$ and $\Psi_1(\dot{\gamma})$). The new function can therefore more accurately fit data even at the low rates of destruction expected in weak shearing flows.

3.2. Strong steady flows

In this Subsection we will consider strong flows, such as extensional deformations, for which the exponential PTT model and its generalisation described here should perform better than the linear one [2]. For that, we will perform a fit to the extensional viscosity data for a melt of polystyrene chains taken from the work of Nielsen et al. [12].

In order to determine the steady unidirectional extensional viscosity $\eta_E = (\tau_{xx} - \tau_{yy})/\dot{\epsilon}$ we consider a velocity field given by $\mathbf{u} = \dot{\boldsymbol{\epsilon}}(x, -y/2, -z/2)$ leading to the following rate of deformation tensor:

$$\mathbf{D} = \dot{\epsilon}\begin{bmatrix}1 & 0 & 0\\ 0 & -1/2 & 0\\ 0 & 0 & -1/2\end{bmatrix}. \tag{22}$$

Here $\dot{\epsilon}$ is the constant imposed elongation rate.

This kinematic field leads to the following nonlinear system of equations for τ_{xx}, τ_{yy} and τ_{zz}:

$$\tau_{xx}\left(\Gamma(\beta)E_{\alpha,\beta}\left(\frac{\varepsilon\lambda}{\eta_p}\tau_{kk}\right) - 2\lambda\dot{\epsilon}(1-\xi)\right) = 2\eta_p\dot{\epsilon}, \tag{23}$$

$$\tau_{yy}\left(\Gamma(\beta)E_{\alpha,\beta}\left(\frac{\varepsilon\lambda}{\eta_p}\tau_{kk}\right) + \lambda\dot{\epsilon}(1-\xi)\right) = -\eta_p\dot{\epsilon}, \tag{24}$$

$$\tau_{zz}\left(\Gamma(\beta)E_{\alpha,\beta}\left(\frac{\varepsilon\lambda}{\eta_p}\tau_{kk}\right) + \lambda\dot{\epsilon}(1-\xi)\right) = -\eta_p\dot{\epsilon}, \tag{25}$$

with $\tau_{kk} = \tau_{xx} + \tau_{yy} + \tau_{zz}$. Solution of this system of equations allows us to determine η_E and its variation with extension rate. One approach to solving (23)–(25) is an iterative approach (e.g. the Newton–Raphson method) but this can be slow. An alternate approach that allows one to easily obtain the extensional viscosity is now given.

Note that the equations for τ_{yy} and τ_{zz} are identical and therefore, $\tau_{kk} = \tau_{xx} + 2\tau_{yy}$. Summing Eqs. (23) + 2 × (24) leads to

$$\tau_{kk}\Gamma(\beta)E_{\alpha,\beta}\left(\frac{\varepsilon\lambda}{\eta_p}\tau_{kk}\right) = N_1 2Wi(1-\xi) \tag{26}$$

with $N_1 = \tau_{xx} - \tau_{yy}$ and $Wi = \lambda\dot{\epsilon}$. Taking the difference of (23) and (24) we obtain:

$$N_1 = 3\eta_p\dot{\epsilon}\left[\frac{\Gamma(\beta)E_{\alpha,\beta}\left(\frac{\varepsilon\lambda}{\eta_p}\tau_{kk}\right)}{\left(\Gamma(\beta)E_{\alpha,\beta}\left(\frac{\varepsilon\lambda}{\eta_p}\tau_{kk}\right) - 2Wi(1-\xi)\right)\left(\Gamma(\beta)E_{\alpha,\beta}\left(\frac{\varepsilon\lambda}{\eta_p}\tau_{kk}\right) + Wi(1-\xi)\right)}\right]. \tag{27}$$

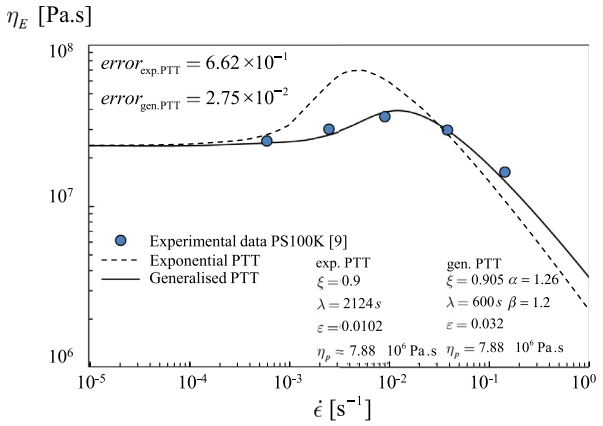

Fig. 4. Fit to the extensional viscosity using the exponential and generalised PTT models. The rheological data was obtained from Nielsen et al. [12] for a polystyrene with a molecular weight of 100 kg/mol.

Let $G = \eta_p/\lambda$, $\widetilde{T} \equiv \frac{\tau_{kk}}{G}$ and $\widetilde{K}(\widetilde{T}) \equiv \Gamma(\beta)E_{\alpha,\beta}(\varepsilon\widetilde{T})$. Division of Eq. (26) by G leads to

$$\frac{N_1}{G} \equiv \widetilde{N} = \frac{\widetilde{T}\widetilde{K}(\widetilde{T})}{2Wi(1-\xi)} \tag{28}$$

and substitution of $\widetilde{N}$ into Eq. (27) divided by G results in the following quadratic equation for $Wi = \lambda\dot{\epsilon}$:

$$a(Wi)^2 + bWi - c = 0, \tag{29}$$

with $a = 2(1-\xi)(3+\widetilde{T}(1-\xi))$, $b = \widetilde{T}\widetilde{K}(1-\xi)$ and $c = \widetilde{T}\widetilde{K}^2$. After solving for $Wi(\widetilde{T})$ we obtain the extensional stress (scaled with G) from Eq. (28), and therefore, the extensional viscosity can be easily calculated as $\eta_E/\eta_0 = \widetilde{N}/Wi = (\tau_{xx}-\tau_{yy})/(\eta_0\dot{\epsilon})$. The idea is to generate a vector of values for $\widetilde{T}$ and subsequently obtain $\widetilde{K}$, $Wi(\widetilde{T})$, $\widetilde{N}(\widetilde{T})$ without the need for iteration.

We have compared this method with the numerical one, and, the latter approach proved to be much faster and reliable (even though the two techniques provide the same results, as expected).

Our common sense tells us that the rate of network destruction in a complex fluid may not always follow a universal exponential behavior because it is both material and topology-dependent and therefore, a generalisation such as the one described here is an empirical but logical increment to the original PTT models.

From the fit shown in Fig. 4 to the polystyrene data of Nielsen et al. [12] we may conclude that the new model allows a much better fit (the mean square error in Fig. 4 is obtained with Eq. (21), adapted to the available data for η_E) to the extensional viscosity obtained for a polystyrene with a molecular weight of 100 kg/mol. The generalised model results in a mean square error that is 24 times smaller than the fitting error obtained for the exponential PTT model. Also note that we obtained AIC values of 173 and 180 for the generalised and exponential models, respectively. Therefore, again the generalised model is the better parsimonious model.

3.3. Unsteady flows

We now investigate the influence of α, β on the normalized transient shear viscosity of a generalised PTT model in start-up for two different Weissenberg numbers of $Wi = \lambda\dot{\epsilon} = 10,\ 100$ (Fig. 5). The trend observed in the viscosity curve by changing both α and β is similar, with the transient shear viscosity, $\eta^+(t,\dot{\gamma})/\eta_p$, increasing with increments in either of these two parameters. The difference is that the increase of β leads to a slower nonlinear increase of η^+.

As the deformation rate decreases, the influence of the parameters α and β on the curve evolution is less pronounced (Fig. 5). Note that increasing the shear rate results in a stronger overshoot being obtained.

In transient extension we obtain a different behavior from that of shear (Fig. 6). The extensional viscosity again increases with time (or strain) until it reaches a steady-state value, but rather than observing a stress overshoot we observe strain-hardening followed by an inflection in the curvature and a monotonic approach to steady state. The influence of α and β is similar to that observed for the transient shear viscosity.

3.4. Fit to experimental data

We will now perform a fit to a complete experimental data set available for a well-characterized LDPE melt (see [14–16] for more details). Data available includes the linear viscoelastic response as well as the transient shear and uniaxial extensional viscosity. Fig. 7 shows the fit to the linear viscoelastic data (storage and loss modulus) considering six discrete relaxation modes to capture the broad relaxation spectrum of the LDPE.

We will now show the fits obtained for transient uniaxial extensional and shear viscosities considering the generalised and exponential PTT models (Fig. 8).

The fits obtained closely follow the trends observed in the experimental data, and the fit obtained for the generalised PTT model is qualitatively good. For the case of extensional viscosity we observe that the generalised model slightly overpredicts the transient experimental data. This deviation is further amplified when considering the exponential model. The fit obtained for transient start-up shear flows is visually better than the one obtained for transient extensional flows, but, at long times the generalised model deviates from the very gradual continued thinning observed in the experiments. Note that with more modes it would be possible to better resolve this thinning effect. For high shear rates the PTT model shows oscillations that were predicted before by Phan–Thien and Tanner [1,2]. Note that a fit to this data was performed in the work of Inkson et al. [16] considering the pom-pom models with 9 modes. By comparing the fits obtained with the two models it is obvious that the generalised model provides a better fit to experimental data. As before, we also compared the AIC values obtained for these two fits and obtained numerical values of 630 and 754 for the generalised and exponential models (transient shear), respectively, and 1643 for the generalised and 1720 for the exponential models (transient extension). Again, the generalised model appears to be a more statistically appropriate model for describing the available data. It should be remarked that an improved fit to the experimental data could be obtained with the exponential model, sacrificing either the shear or the extensional fits. Here we have minimized the overall fitting error by considering both sets of data.

We can therefore conclude that the α and β parameters in the Mittag–Leffler function allow us to increase or decrease the extensional plateau and how it varies with extension rate without significantly affecting the shear viscosity plateau, therefore, incorporating these parameters is imperative when performing a fit to both transient shear and extensional flows.

4. Analytical solution for the generalised PTT model in rectilinear channel/pipe flows

4.1. Derivation of the analytical solution for the generalised simplified PTT model

We will now derive an analytical solution for the fully developed flow of the generalised sPTT model (with the slip parameter in the Gordon–Showalter derivative set to $\xi = 0$) in two-dimensional channel and pipe flows. In order to avoid the introduction of too many equations, we will use a compact notation for both channel and pipe

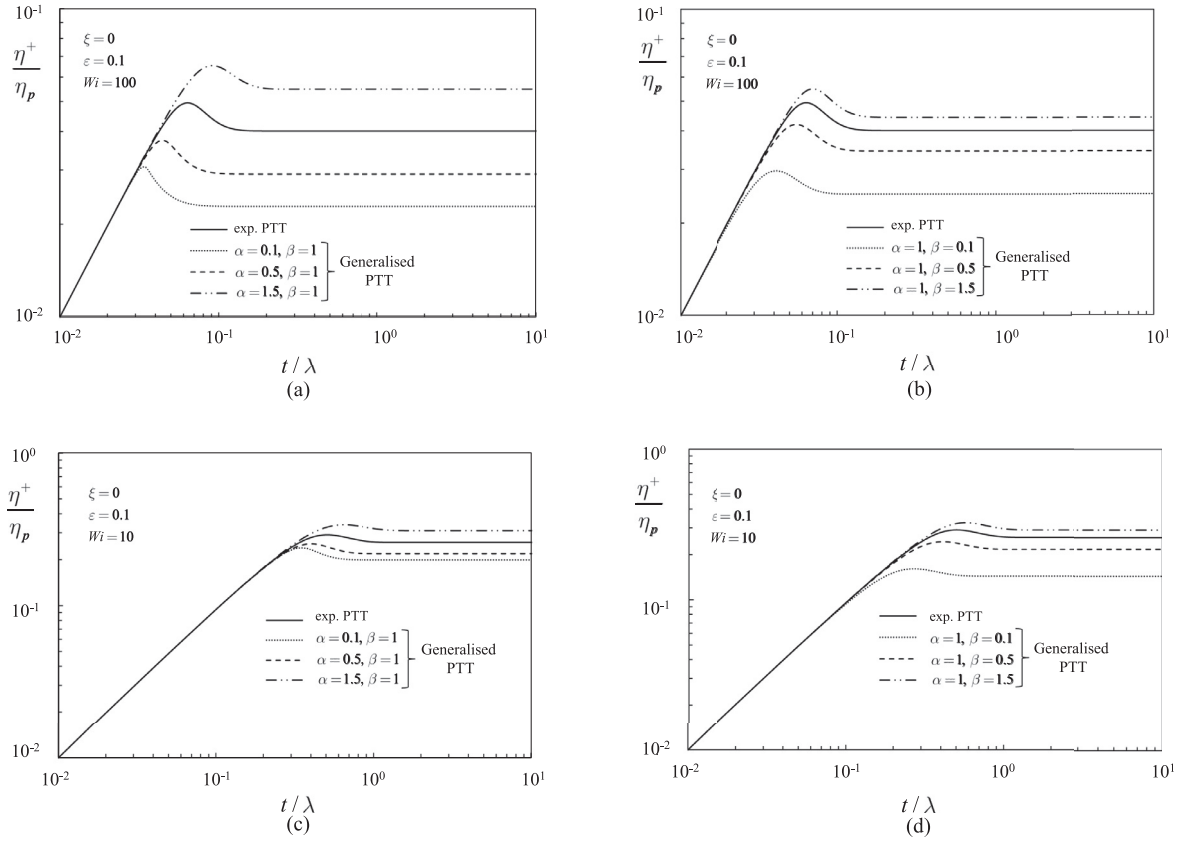

Fig. 5. Normalised transient shear viscosity of a generalised PTT model in start-up for two different Weissenberg numbers and different α, β values. Note that $\xi = 0$.

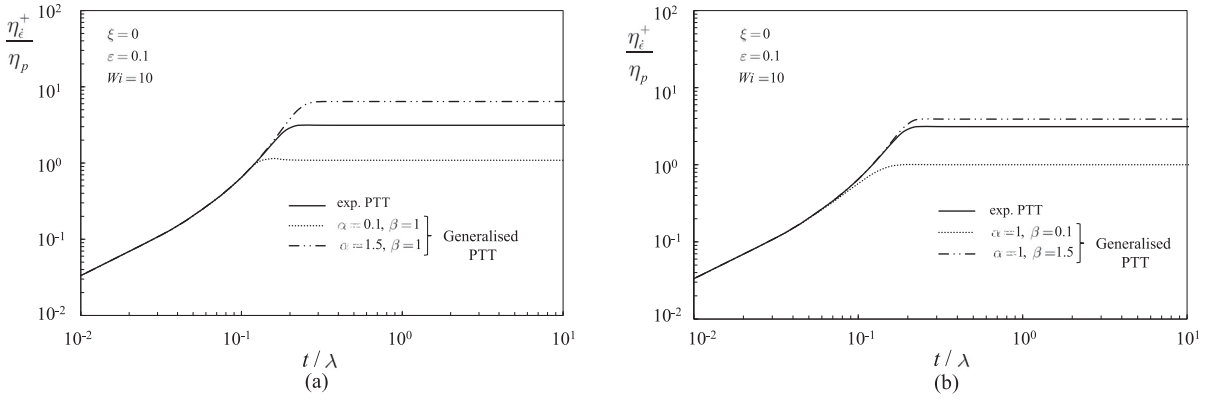

Fig. 6. Normalised transient uniaxial extensional viscosity of a generalised PTT model in start-up for $Wi = 10$ and different α, β values. Note that $\xi = 0$.

geometries (see Fig. 9), where y is the transverse (or radial) direction and $\delta = 0, 1$ stands for channel or pipe flow, respectively [13].

The constitutive equations for the generalised PTT model describing this flow ($\mathbf{u} = \{\dot{\gamma} y, 0, 0\}$ with $\dot{\gamma}(y) = du/dy$), can be further simplified to:

$$K(\tau_{kk})\tau_{xx} = (2 - \xi)(\lambda\dot{\gamma})\tau_{xy} \tag{30}$$

$$K(\tau_{kk})\tau_{yy} = -\xi(\lambda\dot{\gamma})\tau_{xy} \tag{31}$$

$$K(\tau_{kk})\tau_{xy} = \eta_p\dot{\gamma} + \left(1 - \frac{\xi}{2}\right)(\lambda\dot{\gamma})\tau_{yy} - \frac{\xi}{2}(\lambda\dot{\gamma})\tau_{xx} \tag{32}$$

where $\tau_{kk} = \tau_{xx} + \tau_{yy}$ is the trace of the stress tensor in shear flow. Note that the shear rate is no longer a constant, but varies with y. For the generalised sPTT model if we set $\xi = 0$, Eq. (31) then implies $\tau_{yy} = 0$ and thus the trace of the stress tensor becomes $\tau_{kk} = \tau_{xx}$, and the network destruction function becomes an explicit function of the streamwise normal stress $K(\tau_{xx})$. The second normal stress coefficient for the simplified form of the gPTT model is identically zero. Upon division of the expressions for the two nonvanishing components of the stress (30)–(32), $K(\tau_{xx})$ cancels out, and an explicit relationship between the streamwise normal stress and the shear stress is obtained,

$$\tau_{xx} = 2\frac{\lambda}{\eta_p}\tau_{xy}^2 \tag{33}$$

Note that the shear stress can be easily obtained by integration of the momentum equation (11), leading to,

$$\tau_{xy} = P_x\frac{y}{2\delta}, \tag{34}$$

where $P_x = dP/dx < 0$ is the imposed pressure gradient, and is negative in sign. Combining Eqs. (32), (33) and (34) we obtain the velocity

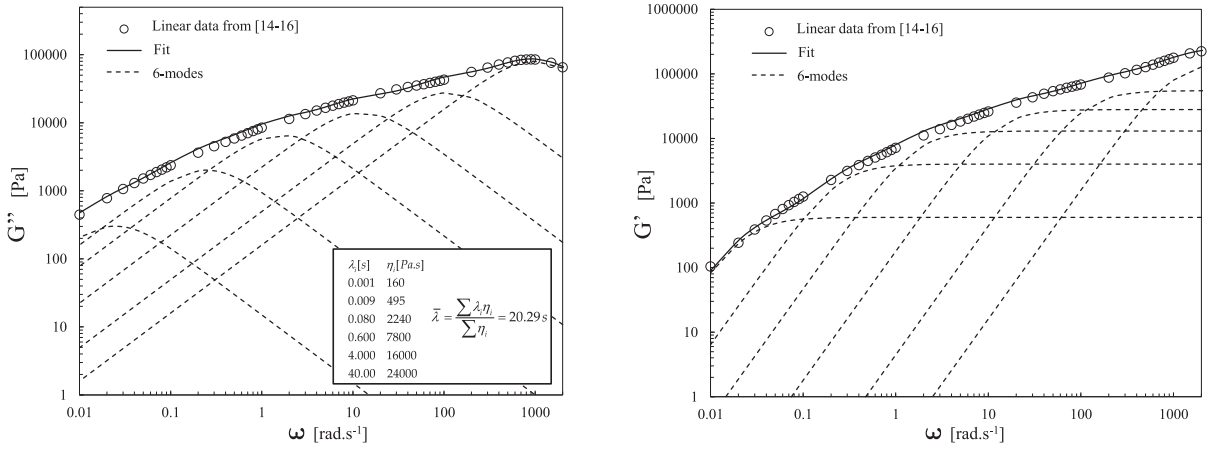

Fig. 7. Multimode fit to the linear viscoelastic data of an LDPE melt [14–16].

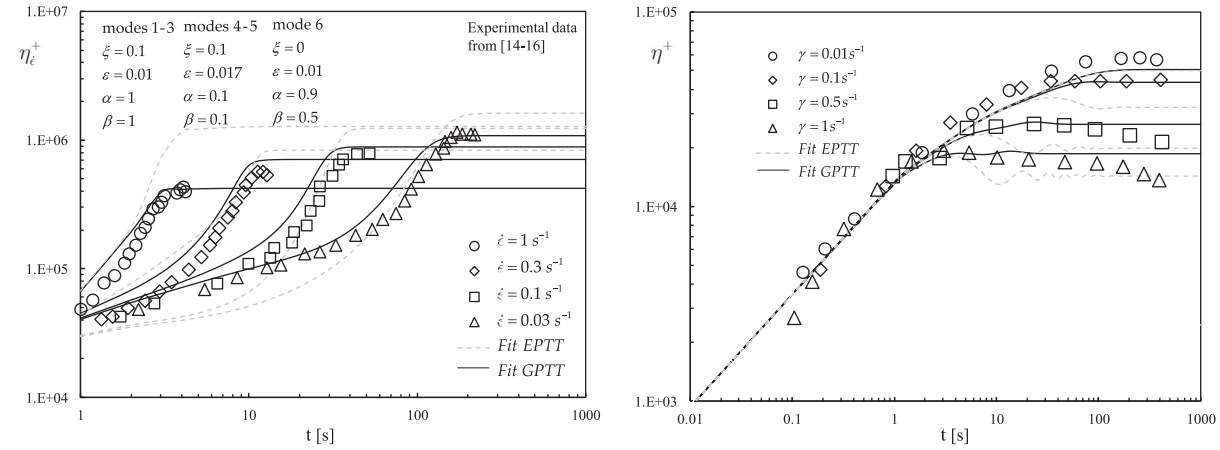

Fig. 8. Fit to the transient uniaxial extensional and shear viscosities of an LDPE [14–16] considering the generalised and exponential PTT models (with 6 modes). For the exponential PTT model we have considered $\xi = 0.1$ and $\varepsilon = 0.01$ for all modes.

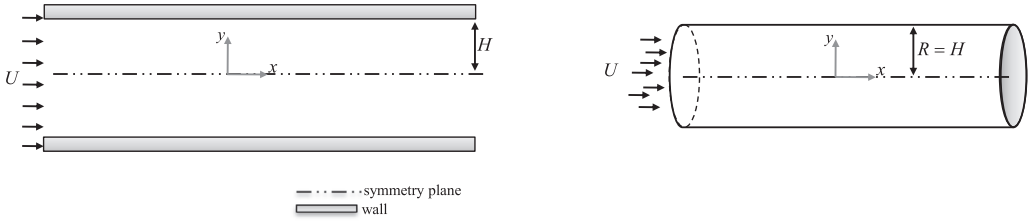

Fig. 9. Channel and pipe geometries.

gradient (for more details on a similar derivation please see [13]):

$$\dot{\gamma}(y) = \Gamma(\beta) E_{\alpha,\beta}\left(\frac{2\varepsilon\lambda^2}{\eta_p^2} P_x^2 \frac{y^2}{2^{2\delta}}\right) \frac{P_x y}{\eta_p 2^{\delta}} \tag{35}$$

The velocity profile can be obtained from integration of the corresponding velocity gradient subjected to the no-slip boundary condition at the bounding walls,

$$u(y) = -\int_y^H \dot{\gamma}(y)dy \tag{36}$$

leading to the following velocity profile:

$$u(y) = \frac{\Gamma(\beta) P_x}{\eta_p 2^{\delta}} \sum_{k=0}^{\infty}\left(\frac{1}{2k+2}\left(\frac{2\varepsilon\lambda^2 P_x^2}{\eta_p^2 2^{2\delta}}\right)^k\right)\left(\frac{y^{2k+2} - H^{2k+2}}{\Gamma(\alpha k+\beta)}\right). \tag{37}$$

Note that this velocity profile depends on the imposed pressure gradient. If we set the constraint of a specified flow rate, we may obtain the corresponding pressure gradient by solving the following equation:

$$U = \frac{1}{H^{\delta+1}} \int_0^H 2^{\delta} y^{\delta} u(y) dy \tag{38}$$

which results in the following nonlinear equation for the channel geometry,

$$\frac{-P_x \Gamma(\beta)}{H\eta_p} \sum_{k=0}^{\infty}\left(\frac{1}{2k+2}\left(\frac{2\varepsilon\lambda^2 P_x^2}{\eta_p^2}\right)^k\right)\left(\frac{H^{2k+3}}{\Gamma(\alpha k+\beta)}\right)\left(\frac{2k+2}{2k+3}\right) - U = 0, \tag{39}$$

and for the pipe geometry:

$$\frac{-P_x\Gamma(\beta)}{2H^2\eta_p}\sum_{k=0}^{\infty}\left(\frac{1}{2k+2}\left(\frac{2\varepsilon\lambda^2P_x^2}{4\eta_p^2}\right)^k\right)\left(\frac{H^{2k+4}}{\Gamma(\alpha k+\beta)}\right)\left(\frac{k+1}{k+2}\right)-U=0. \quad (40)$$

If the pressure gradient P_x is specified, Eq. (39) or (40) allow the calculation of the average velocity in the duct or pipe, respectively, and Eq. (37) can be used to evaluate the full velocity profile.

The equations for the velocity and pressure can also be written in dimensionless form as:

$$\bar{u}(\bar{y})=\Gamma(\beta)\bar{P}_x\sum_{k=0}^{\infty}\left(\frac{1}{2k+2}\left(2\varepsilon(Wi)^2\bar{P}_x^2\right)^k\right)\left(\frac{1-\bar{y}^{2k+2}}{\Gamma(\alpha k+\beta)}\right). \quad (41)$$

$$\frac{\Gamma(\beta)\bar{P}_x}{2}\sum_{k=0}^{\infty}\left(\frac{1}{2k+2}\left(\frac{2\varepsilon(Wi)^2\bar{P}_x^2}{4}\right)^k\right)\left(\frac{k+1}{\Gamma(\alpha k+\beta)(k+2)}\right)-1=0. \quad (42)$$

respectively, with $\bar{y}=y/H$, $\bar{u}=u/U$, $\bar{P}_x=-P_xH^2/(\eta_pU)$ and $Wi=\lambda U/H$.

4.2. Derivation of a semi-analytical solution for the generalised full PTT model

By following the work of [10], one can easily obtain an explicit expression for the shear rate:

$$\dot{\gamma}(y)=\frac{AE_{\alpha,\beta}\left(\Upsilon^{-1}w(y)\right)w(y)}{y} \quad (43)$$

where $A=\Gamma(\beta)\eta_p2^\delta/(2\lambda^2\xi(2-\xi)P_x)$, $\Upsilon=\xi(2-\xi)/(\varepsilon(1-\xi))$, $w(y)=1-\sqrt{1-(ay)^2}$ and $a=-2^{1-\delta}\lambda P_x\sqrt{\xi(2-\xi)}\eta_p^{-1}$.

Using the definition of $E_{\alpha,\beta}$ from Eq. (4) we obtain:

$$\dot{\gamma}(y)=A\left(\frac{w(y)}{\Gamma(\beta)y}+\frac{\Upsilon^{-1}w(y)^2}{\Gamma(\alpha+\beta)y}+\frac{\Upsilon^{-2}w(y)^3}{\Gamma(2\alpha+\beta)y}+\ldots+\frac{\Upsilon^{-k}w(y)^{k+1}}{\Gamma(k\alpha+\beta)y}+\ldots\right) \quad (44)$$

and therefore, from Eq. (36) we have

$$u(y)=A\sum_{k=0}^{\infty}\frac{(-1)^{k+1}\Upsilon^{-k}}{\Gamma(k\alpha+\beta)}\int_y^H\frac{w(y)^{k+1}}{y}dy \quad (45)$$

The integral $\int\frac{w(y)^{k+1}}{y}dy$ can be easily obtained by considering the substitutions $u=\sqrt{1-(ay)^2}$ and $v=u+1$ leading to an integral of the final compound form $\int\frac{(v-2)^k(v-1)}{v}dv$. Using the binomial expansion we arrive at the final expression for the velocity profile:

$$u(y)=A\sum_{k=0}^{\infty}\left(\frac{(-1)^{k+1}\Upsilon^{-k}}{\Gamma(k\alpha+\beta)}\left[\chi(H)-\chi(y)\right]\right) \quad (46)$$

with

$$\chi(y)=\left[\sum_{n=1}^{k}\binom{k}{n}(-2)^{k-n}\left(\frac{(v(y))^{n+1}}{n+1}-\frac{(v(y))^n}{n}\right)+(-2)^k\left(v(y)-\log((v(y)))\right)\right]. \quad (47)$$

and $v(y)=1+\sqrt{1-(ay)^2}$.

Finally the pressure gradient P_x (contained within the parameter A) can be obtained once again by imposing a certain flow rate Q (and therefore the velocity U is known), leading to the following integral equation:

$$\begin{aligned}U&=\frac{2^\delta}{H^{\delta+1}}\int_0^H y^\delta A\sum_{k=0}^{\infty}\left[\frac{(-1)^{k+1}\Upsilon^{-k}}{\Gamma(k\alpha+\beta)}(\chi(H)-\chi(y))\right]dy\\&=2^\delta A\sum_{k=0}^{\infty}\left[\frac{(-1)^{k+1}\Upsilon^{-k}}{\Gamma(k\alpha+\beta)}\chi(H)\right]-\frac{2^\delta A}{H^{\delta+1}}\sum_{k=0}^{\infty}\left[\frac{(-1)^{k+1}\Upsilon^{-k}}{\Gamma(k\alpha+\beta)}\int_0^H y\chi(y)dy\right]\\&=2^\delta A\sum_{k=0}^{\infty}\left[\frac{(-1)^{k+1}\Upsilon^{-k}}{\Gamma(k\alpha+\beta)}\chi(H)\right]-\delta\frac{2^\delta A}{H^{\delta+1}a^2}\sum_{k=0}^{\infty}\left[\frac{(-1)^{k+1}\Upsilon^{-k}}{\Gamma(k\alpha+\beta)}(\Omega_1(H)-\Omega_1(y))\right]\\&\quad-\delta\frac{2^\delta AH^2}{H^{\delta+1}}\sum_{k=0}^{\infty}\left[\frac{(-1)^{k+1}\Upsilon^{-k}}{\Gamma(k\alpha+\beta)}(\Theta_1(H)-\Theta_1(y))\right]\\&\quad-(1-\delta)\frac{2^\delta AH}{H^{\delta+1}}\sum_{k=0}^{\infty}\left[\frac{(-1)^{k+1}\Upsilon^{-k}}{\Gamma(k\alpha+\beta)}(\Omega_0(H)-\Omega_0(y))\right]\\&\quad-(1-\delta)\frac{2^\delta AH}{H^{\delta+1}}\sum_{k=0}^{\infty}\left[\frac{(-1)^{k+1}\Upsilon^{-k}}{\Gamma(k\alpha+\beta)}(\Theta_0(H)-\Theta_0(y))\right]\end{aligned} \quad (48)$$

where

$$\Omega_1(y)=\left[\sum_{n=1}^{k}\binom{k}{n}(-2)^{k-n}\left[\frac{1}{n+1}\left(\frac{(v(y))^{n+2}}{n+2}-\frac{(v(y))^{n+3}}{n+3}\right)-\frac{1}{n}\left(\frac{(v(y))^{n+1}}{n+1}-\frac{(v(y))^{n+2}}{n+2}\right)\right]\right], \quad (49)$$

$$\Theta_1(y)=\left[\frac{(-2)^k}{H^2}\left(\frac{y^2}{4}+\frac{y^2\log(v(y))}{2}-\frac{\sqrt{1-(ay)^2}(4a^2y^2-10)}{12a^2}\right)\right], \quad (50)$$

$$\begin{aligned}\Omega_0(y)&=\sum_{n=1}^{k}\binom{k}{n}\frac{(-2)^{k-n}}{H}\frac{1}{n+1}\left[y+\sum_{l=1}^{n+1}\binom{n+1}{l}\frac{1}{a}\int_{y=0}^{y=H}(\cos(u))^l du\right],\\&\quad-\frac{1}{n}\sum_{n=1}^{k}\binom{k}{n}\frac{(-2)^{k-n}}{H}\left[y+\sum_{l=1}^{n}\binom{n}{l}\frac{1}{a}\int_{y=0}^{y=H}(\cos(u))^l du\right]\end{aligned} \quad (51)$$

with $u=\arcsin(ay)$, $dy=\cos(u)/a\ du$ and $\int(\cos(u))^j du=\frac{j-1}{j}\int(\cos(u))^{j-2}du+\frac{(\cos(u))^{j-1}\sin(u)}{j}$.

$$\Theta_0(y)=\left[\frac{(-2)^k}{H}\left(\frac{3\arcsin(ay)}{2a}+\frac{y\sqrt{1-(ay)^2}}{2}+y\log(v)\right)\right]. \quad (52)$$

These equations can also be written in dimensionless form, leading to:

$$\begin{aligned}1&=\frac{2^\delta A}{U}\sum_{k=0}^{\infty}\left[\frac{(-1)^{k+1}\Upsilon^{-k}}{\Gamma(k\alpha+\beta)}\chi(H)\right]\\&\quad-\delta\frac{2A}{UH^2a^2}\sum_{k=0}^{\infty}\left[\frac{(-1)^{k+1}\Upsilon^{-k}}{\Gamma(k\alpha+\beta)}(\Omega_1(H)-\Omega_1(y))\right]\\&\quad-\delta\frac{2A}{U}\sum_{k=0}^{\infty}\left[\frac{(-1)^{k+1}\Upsilon^{-k}}{\Gamma(k\alpha+\beta)}(\Theta_1(H)-\Theta_1(y))\right]\\&\quad-(1-\delta)\frac{2A}{U}\sum_{k=0}^{\infty}\left[\frac{(-1)^{k+1}\Upsilon^{-k}}{\Gamma(k\alpha+\beta)}(\Omega_0(H)-\Omega_0(y))\right]\\&\quad-(1-\delta)\frac{2A}{U}\sum_{k=0}^{\infty}\left[\frac{(-1)^{k+1}\Upsilon^{-k}}{\Gamma(k\alpha+\beta)}(\Theta_0(H)-\Theta_0(y))\right]\end{aligned} \quad (53)$$

where $\frac{A}{U}=-\frac{\Gamma(\beta)2^\delta}{2\xi(2-\xi)\overline{P}_x(W_i)^2}$ and $aH=2^{1-\delta}\overline{P}_xWi\sqrt{\xi(2-\xi)}$.

Note that the exponential PTT model is recovered when $\alpha=\beta=1$. For the linear PTT model we have to solve the following equations for channel and pipe, respectively [10]:

$$\frac{3}{\overline{P}_x}=\frac{6}{(aH)^2}\left[1+\frac{2\varepsilon(1-\xi)}{\xi(2-\xi)}\right]\left(1-\frac{\pi}{4aH}+\frac{1}{2aH}\arctan\left(\frac{\sqrt{1-a^2H^2}}{aH}\right)-\frac{\sqrt{1-a^2H^2}}{2}\right)-\frac{2\varepsilon(1-\xi)}{\xi(2-\xi)} \quad (54)$$

$$\frac{8}{\overline{P}_x}=\frac{4}{(aH)^2}\left[1+\frac{2\varepsilon(1-\xi)}{\xi(2-\xi)}\right]\left(1-\frac{2}{3}\sqrt{1-a^2H^2}-\frac{2}{3}\frac{(1-\sqrt{1-a^2H^2})}{a^2H^2}\right)-\frac{2\varepsilon(1-\xi)}{\xi(2-\xi)} \quad (55)$$

The nonlinear equation for the pressure gradient, Eq. (48), is solved numerically, using the Newton–Raphson method, and a finite number

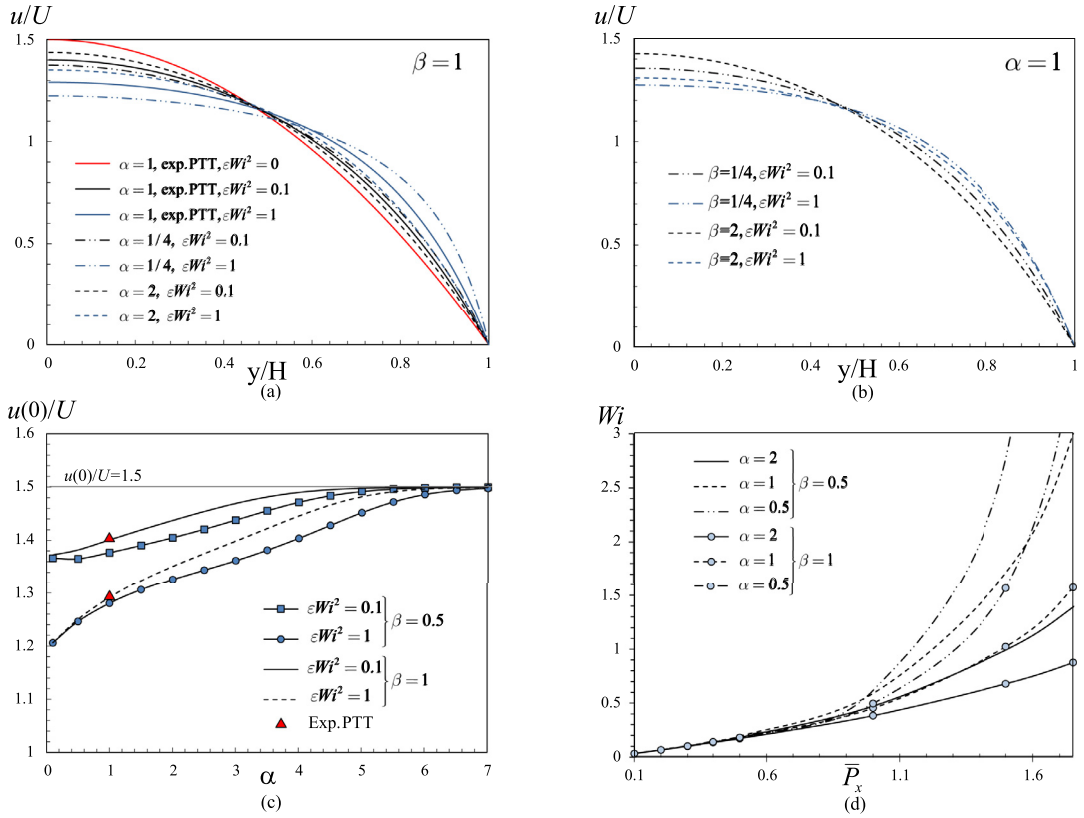

Fig. 10. Velocity profiles obtained for pressure-driven channel flow considering different values of εWi^2 and different values of α and β. Comparison with the exponential PTT model. (a) $\beta = 1$, (b) $\alpha = 1$. (c) Variation of the dimensionless centerplane velocity with changes in α and β. (d) Variation of the dimensionless flow rate (Wi) with the dimensionless pressure gradient ($\bar{P}_x = -P_x H^2/(\eta_p U)$) for different values of α and β.

of terms in the series expansion. Care should be taken when solving this equation because the number of terms considered will influence the final solution. We increased that number progressively until reaching a stable and accurate solution (this will be explained in detail in the next susbsection). Determination of the pressure gradient then allows us to obtain the velocity profile using Eq. (46). It should be pointed out that even without these series expansions for velocity and pressure gradient, Eqs. (34)–(36) and (38) together allow us to obtain the shear rate, velocity profile and flow rate, that is, $\dot{\gamma}(y)$, $u(y)$ and Q, respectively, from a specified value of the pressure gradient.

4.3. The influence of the Mittag–Leffler function on the velocity and stress profiles

In this subsection we investigate the influence of the Mittag–Leffler function on the velocity and stress profiles, studying the influence of α and β on the velocity profile for channel and pipe flows and comparing these results with the exponential PTT model, whose analytical solution is given in the work of Oliveira and Pinho [13].

It should be remarked that although the solutions are given in a series form, it was observed that for the range of Wi numbers considered, a sum of up to 100 terms proved to be sufficient to obtain accurate results (a normalized relative error between subsequent computations below 10^{-7}). Some of these computations took less than a second (we provide as supplementary material the codes used to compute velocity and pressure profiles).

Fig. 10 shows the velocity profiles obtained for channel flow considering different Wi and different values of α and β. The case of pipe flow will not be addressed here since this was previously considered extensively in the work of Oliveira and Pinho [13] for the case of linear and exponential PTT models.

From Fig. 10(a) we conclude that increasing the parameter α ($\alpha > 1$) provides a more shear thinning non-Newtonian velocity profile (in the sense that an increase of elasticity would lead to a more flattened bulk velocity profile in comparison with the exponential PTT model). For $\alpha < 1$ this effect is even more pronounced, resulting in smaller center velocity profile values. In Fig. 10(b) we perform a comparison between different generalised PTT model parameter values, by keeping constant $\alpha = 1$ and varying εWi^2 and β. We conclude that a decrease in β leads to a decrease of the centerplane velocity, resulting also in a more flattened velocity profile.

Although not shown in Fig. 10, we find that for the same pressure gradient and $\alpha = 1$ we obtain a higher flow rate for the generalized PTT model (in comparison with the exponential PTT model) for $\beta < 1$ and a lower flow rate for $\beta > 1$. The same conclusion is obtained when $\beta = 1$ is fixed and we vary α. This result makes sense from examination of Fig. 2; we see that the rate of destruction of chains increases for lower α and β, and therefore facilitates the production of short chain segments that have been removed from the polymer network.

Since the stress profiles are dependent on the pressure gradient, see Eqs. (33) and (34), their increase/decrease (in absolute value) is directly related to the increase/decrease (in absolute value) of the pressure gradient. To see the stress profiles for the cases of linear and exponential PTT model, please consult [13].

Fig. 10(c) shows the variation of the normalized centerplane velocity with α and β, and with the flow strength, given by the parameter εWi^2. We observe that the centreplane velocity increases with both α and β, and for high α values we reach the maximum centerplane velocity obtained for the Newtonian and Upper–Convected Maxwell (UCM) profiles (1.5U). As shown in Fig. 2(a) for large values of α we need very high ε values to see any change in the destruction rate and therefore, the UCM model is recovered. In the limit $\varepsilon Wi^2 \to 0$ we recover the

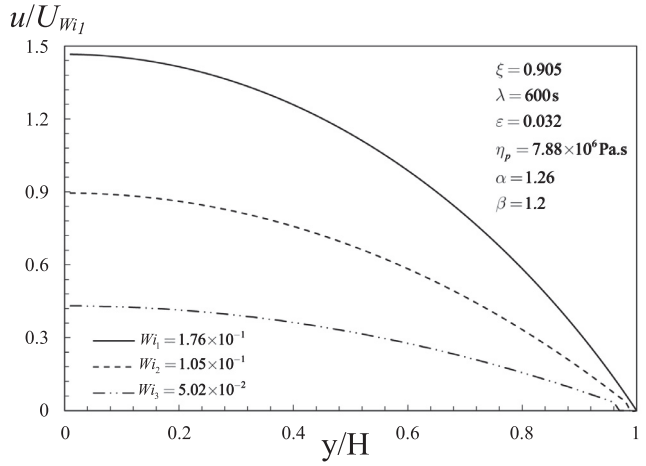

Fig. 11. Velocity profiles obtained for pipe flow considering the parameters obtained for the fit to the rheological data obtained from Nielsen et al. [12] for a polystyrene PS100K (see Fig. 4).

Newtonian fluid and a progressively more flattened profile is obtained for higher εWi^2.

Finally, Fig. 10(d) shows the variation of the dimensionless flow rate through the channel (given by $Wi = \lambda U/H^{1+\delta} = \lambda Q/H^{2+\delta}$) with the normalized pressure gradient. For a low pressure gradient (the limit of creeping flows) we obtain low Wi values, reaching the Newtonian (linear) limit. As the dimensionless pressure gradient increases and shear thinning becomes important, the Weissenberg number increases more rapidly as expected. Note that the decrease of both α and β leads to an increase of Wi. This happens because, in each case, we have an increase in the destruction rate of the chains and thus a progressive decrease in the polymeric network stress at high Wi.

Fig. 11 shows the velocity profiles obtained for pipe flow considering the parameters obtained for the fit to the rheological data obtained from Nielsen et al. [12] for a polystyrene PS100K (see Fig. 4). Note that the constitutive flow instability reported in the work of Alves et al. [10] for the exponential PTT model also applies here, and therefore, we must have $ay \leq 1$ in Eq. (46) in order to obtain a real solution. Note that $ay = -2^{1-\delta}\lambda P_x\sqrt{\xi(2-\xi)}\eta_p^{-1}y = aH\bar{y} = b\bar{y}$. Therefore we must have $b \leq 1$ (since $0 \leq \bar{y} \leq 1$), meaning that:

$$Wi\bar{P}_x \leq \frac{1}{2^{1-\delta}\sqrt{\xi(2-\xi)}}. \tag{56}$$

For the particular parameters obtained for the fit shown in Fig. 4 (gen. PTT model with $\delta = 1$ and $\xi = 0.905$), this forces the following restriction $Wi\bar{P}_x \leq 1.00454$.

Fig. 11 shows three velocity profiles obtained for different values of Wi. Note that the Weissenberg number Wi can only be obtained a posteriori because the mean velocity U is not known before the calculations are performed, therefore we impose a pressure gradient $-P_x$ and obtain Wi using Eq. (56). While varying the dimensional pressure gradient, the flow rate will also vary, therefore, the maximum mean velocity obtained over all three cases, denoted by U_{Wi_1} (mean velocity obtained for $Wi_1 = \lambda U_1/H$), is used to normalize the velocity profiles in Fig. 11, so that they can be compared directly. We observe that the flow rate increases monotonically with Wi, as expected.

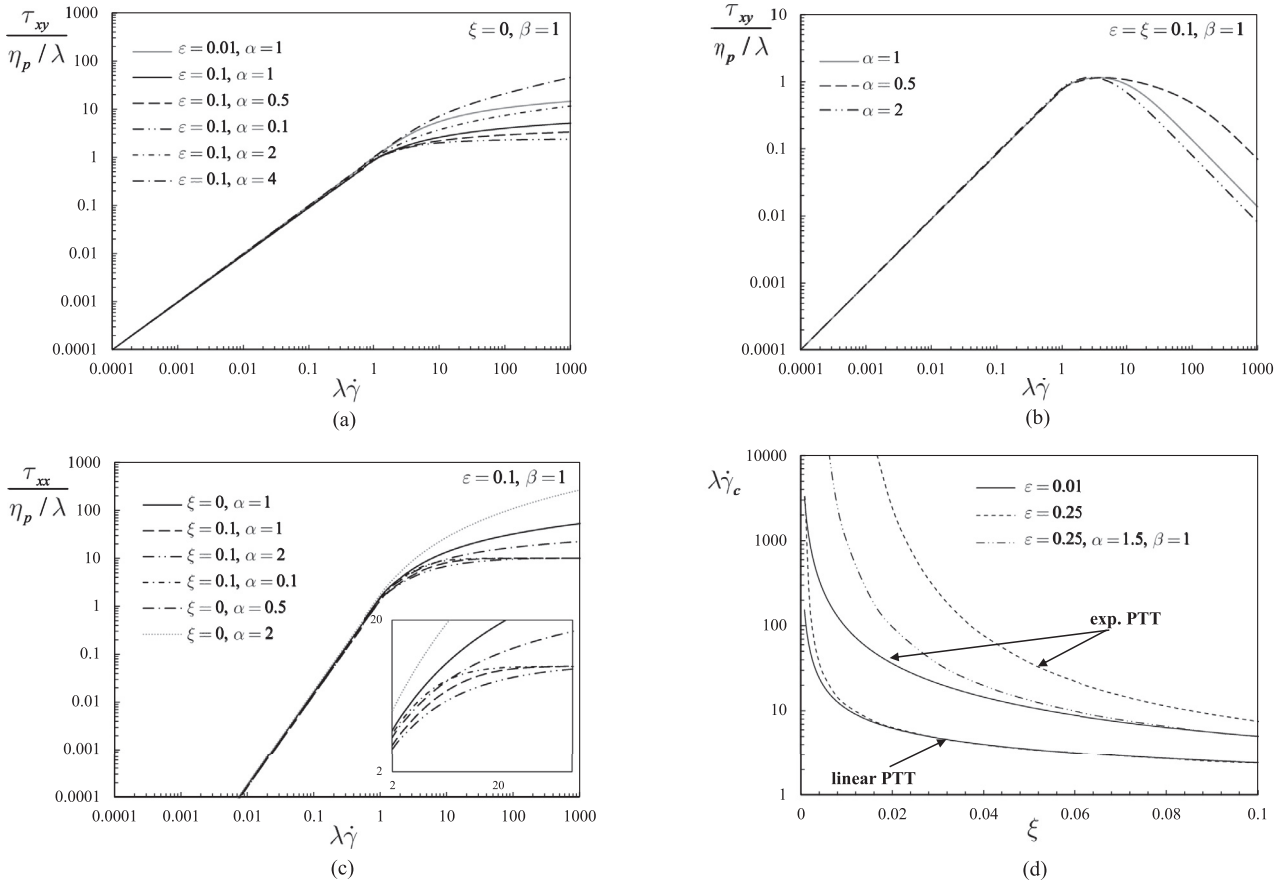

Fig. 12. (a) Variation of the normalized shear stress with $\lambda\dot{\gamma}$ for $\xi = 0$. (b) Variation of the normalized shear stress with $\lambda\dot{\gamma}$ for $\xi \neq 0$. (c) Variation of the normalized normal stress component τ_{xx} with $\lambda\dot{\gamma}$ for different ξ values. (d) Variation of the normalized critical shear rate $\lambda\dot{\gamma}_c$ (the point where the shear stress attains its maximum value) with ξ.

5. Constitutive instability

In this Section we study some of the *stability characteristics* of the model. Namely the fact that pronounced shear thinning is observed in both the steady shear viscosity and first normal stress difference coefficient, and there can be non-monotonic behavior of the shear stress above a certain critical shear rate. Representative results are shown for three variants of the PTT model, namely the linear, exponential and generalized versions. Since closed form analytical expressions are only possible for the linear model (as discussed in detail in [10]), the results are obtained numerically and plotted for different values of the model parameters.

Fig. 12 shows the variation of the normalized shear and normal stresses with the normalized shear rate, together with the variation of the critical Weissenberg number ($Wi_c = \lambda\dot{\gamma}_c$) with ξ.

Fig. 12 (a) shows that a monotonic behavior is observed for the variation of the normalized shear stress with Wi, for both the exponential and generalised PTT models when $\xi = 0$. Note the increase in shear stress with the decrease of ε (the parameter which controls the extensional properties of the model). Note also that for the generalised model we have two additional parameters, α and β. We considered $\beta = 1$ and varied α. For $\alpha < 1$ the shear stress increases linearly at low Wi, and then plateaus for $Wi \gg 1$. For $\alpha > 1$ the rate of increase in the shear stress is higher than the value obtained for the exponential PTT model. In Fig. 12(b) we show the influence of α when $\xi \neq 0$. For this case we obtain a non-monotonic behavior of the shear stress and an unphysical decrease in the stress beyond a certain critical shear rate. This non-monotonicity would lead to a constitutive instability in numerical simulations [17]. For low α values we obtain a more moderate transition while for high α values this transition becomes more abrupt.

As observed by Alves et al. [10] for the linear PTT model, and shown in Fig. 12(c), the scaled normal stress will tend to a constant value (regardless of the value of ξ). Again, we kept $\beta = 1$ and varied α. We observe that a high value of α smooths the variation of the normal stress.

It is interesting to explore the variation with ξ of the normalized critical shear rate ($\lambda\dot{\gamma}_c$) for the different versions of the PTT model. These results are shown in Fig. 12(d). We observe that the exponential and generalised PTT models *delay* the appearance of a maximum shear stress (when compared to the linear model), allowing a wider range of shear rates to be attained before the onset of instability. Note that in the work of Alves et al. [10] a closed form analytical expression is derived for the relationship between the critical Weissenberg number ($\lambda\dot{\gamma}_c$) and both ξ and ε. The same relationship was shown to be the origin of unstable solutions (constitutive instabilities) for pipe and channel flows.

By looking at Eq. (43) one can easily obtain the maximum shear rate at the wall. It turns out that this maximum critical shear rate for a duct flow is given by:

$$\lambda\dot{\gamma}_{\max,c} = \frac{\Gamma(\beta)}{\sqrt{\xi(2-\xi)}} E_{\alpha,\beta}\left(\frac{\varepsilon(1-\xi)}{\xi(2-\xi)}\right) \tag{57}$$

which is the same as shown in Fig. 12(d), for the case of simple shear flow. Above this maximum shear rate, the solutions are complex-valued, and lead to unphysical results.

6. Conclusions

We have proposed a new generalised PTT model that allows a much better fit to rheological data obtained for entangled polymer melts and solutions in both weak shearing and strong elongational flows. The new functional form incorporates the generalised Mittag–Leffler function, providing this new model with up to two additional extra constitutive parameters. Evaluation of the Akaike Information–Criterion (AIC) for fits of the new model to several sets of rheological data show that incorporation of these additional parameters is statistically justified and still results in a suitably parsimonious constitutive model. We have also derived new analytical and semi-analytical solutions for steady fully-developed flows in channels and pipes. This additional constitutive flexibility allows us to describe both steady shear and extensional flows with improved fidelity using only one single relaxation mode and 6 total model parameters η, λ, ε, α, β (plus ξ if a non-zero second normal stress difference is important), in our generalised simplified PTT model.

The gPTT model is already implemented in rheoTool (a toolbox to simulate generalised Newtonian and viscoelastic fluid flows in OpenFOAM® - https://github.com/fppimenta/rheoTool) and also in HiGFlow (a solver based on a finite difference method with meshless interpolation for fluid flow simulations in non-graded hierarchical grids [18]).

Acknowledgments

A.M. Afonso acknowledge the support by CEFT (Centro de Estudos de Fenómenos de Transporte) and through Project PTDC/EMS-ENE/3362/2014 and POCI-01-0145-FEDER-016665 - funded by FEDER funds through COMPETE2020 - Programa Operacional Competitividade e Internacionalização (POCI) and by national funds through FCT - Fundação para a Ciência e a Tecnologia, I.P.

L.L. Ferrás would also like to thank FCT for financial support through the scholarship SFRH/BPD/100353/2014 and project UID-MAT-00013/2013.

M.L. Morgado aknowledges the financial support of FCT through the project UID/Multi/04621/2019 of CEMAT/IST-ID, Center for Computational and Stochastic Mathematics, Instituto Superior Técnico, University of Lisbon.

This work was partially supported by the Fundação para a Ciência e a Tecnologia, I.P. (Portuguese Foundation for Science and Technology) through the project UID/MAT/00297/2019 (Centro de Matemática e Aplicações).

Supplementary material

Supplementary material associated with this article can be found, in the online version, at doi:10.1016/j.jnnfm.2019.06.001.

References

[1] N. Phan-Thien, R.I. Tanner, New constitutive equation derived from network theory, J. Non-Newton Fluid Mech. 2 (1977) 353–365.
[2] N. Phan-Thien, A nonlinear network viscoelastic model, J. Rheol. 22 (1978) 259–283.
[3] R.I. Tanner, R.R. Huilgol, On a classification scheme for flow fields rheol, Acta 14 (1975) 959–962.
[4] L. Ferrás, N.J. Ford, M.L. Morgado, M. Rebelo, G.H. McKinley, J.M. Nóbrega, A primer on experimental and computational rheology with fractional viscoelastic constitutive models, in: AIP Conference Proceedings (Vol. 1843, No. 1, p. 020002), AIP Publishing, 2017.
[5] R. Metzler, J. Klafter, From stretched exponential to inverse power-law: fractional dynamics, cole-cole relaxation processes, and beyond, J. Non-Crystalline Solids 305 (2002) 81–87.
[6] I. Podlubny, Fractional Differential Equations: an Introduction to Fractional Derivatives, Fractional Differential Equations, to Methods of their Solution and Some of their Applications. Vol. 198, Elsevier, 1998.
[7] H. Akaike, Information theory and an extension of the maximum likelihood principle, in: B.N. Petrov, F. Csáki (Eds.), 2nd International Symposium on Information Theory, Tsahkadsor, Armenia, USSR, September 2–8, Akadémiai Kiadó, Budapest, 1971, pp. 267–281.
[8] H. Akaike, A new look at the statistical model identification, IEEE Trans. Autom. Control 19 (1974) 716–723.
[9] K.P. Burnham, D.R. Anderson, Model Selection and Multimodel Inference: a Practical Information-Theoretic Approach, Springer Science & Business Media, 2003.
[10] M.A. Alves, F.T. Pinho, P.J. Oliveira, Study of steady pipe and channel flows of a single-mode Phan-Thien - Tanner fluid, J. Non-Newtonian Fluid Mech. 101 (2001) 55–76.
[11] L.M. Quinzani, R.C. Armstrong, R.A. Brown, Birefringence and laser-doppler velocimetry (LDV) studies of viscoelastic flow through a planar contraction, J. Non-Newtonian Fluid Mech. 52 (1994) 1–36.

[12] J.K. Nielsen, H.K. Rasmussen, O. Hassager, G.H. McKinley, Elongational viscosity of monodisperse and bidisperse polystyrene melts, J. Rheol. 50 (2006) 453–476.
[13] P.J. Oliveira, F.T. Pinho, Analytical solution for fully developed channel and pipe flow of phan-thien - tanner flids, J. Fluid Mech. 387 (1999) 271–280.
[14] J. Meissner, Basic parameters, melt rheology, processing and end use properties of three similar low density polyethylene samples, Pure Appl. Chem. 42 (1975) 553–612.
[15] H.M. Laun, H.M. Münstedt, Elongational behavior of a low density polyethylene melt 1, Rheol. Acta 17 (1978) 415–425.
[16] N.J. Inkson, T.C.B. McLeish, O.G. Harlen, D.J. Groves, Predicting low density polyethylene melt rheology in elongational and shear flows with “pom-pom” constitutive equations, J. Rheol. 43 (1999) 873–896.
[17] R.R. Huilgol, N. Phan-Thien, Fluid Mechanics of Viscoelasticity: General Principles, Constitutive Modelling, Analytical and Numerical Techniques, Elsevier, Amsterdam, 1997.
[18] F.S. Sousaa, C.F.A. Lages, J.L. Ansoni, A. Castelo, A. Simao, A finite difference method with meshless interpolation for fluid flow simulations in non-graded hierarchical grids, 2019 submitted to Journal of Computational Physics.